Spatio-temporal evolution of the dust particle size distribution in dusty argon rf plasmas

Carsten Killer, Matthias Mulsow, and André Melzer
Institut für Physik, Ernst-Moritz-Arndt-Universität Greifswald, 17489 Greifswald, Germany

An imaging Mie scattering technique has been developed to measure the spatially resolved size distribution of dust particles in extended dust clouds. For large dust clouds of micron-sized plastic particles confined in an rf discharge, a segmentation of the dust cloud into populations of different sizes is observed, even though the size differences are very small. The dust size dispersion inside a population is much smaller than the difference between the populations. Furthermore, the dust size is found to be constantly decreasing over time while the particles are confined in an inert argon plasma. The processes responsible for the shrinking of the dust in the plasma have been addressed by mass spectrometry, *ex situ* microscopy of the dust size, dust resonance measurements, *in situ* determination of the dust surface temperature and FT-IR absorption. It is concluded that both a reduction of dust size and its mass density due to outgassing of water and other volatile constituents as well as chemical etching by oxygen impurities are responsible for the observations.

I. INTRODUCTION

In all dusty plasmas, the dust particle size is a crucial parameter, since all forces acting on a dust particle depend on its size (here denoted by the radius a). The gravitational force is proportional to a^3 and therefore only significant for particles with a size of at least a few 100 nm. The electric field force is proportional to the dust charge, which is generally assumed to scale linearly with the radius a. Drag forces like the neutral drag, ion drag, radiation pressure or the thermophoretic force are proportional to a^2 [1].

Low temperature plasmas containing dust particles are widely studied for fundamental research as well as technological applications [1, 2]. In many technological processing plasmas, dust particles grow from sputtered material or due to chemically reactive plasma constituents [3]. The formation of dust in these plasmas can severely influence the plasma conditions and therefore disturbs the plasma processing [4, 5]. In other situations, dust growth can be useful and is employed e.g. to improve the efficiency of polymorphous silicon solar cells [6].

In early experiments on the dust formation in plasmas, the particles were detected and studied *in situ* by laser light scattering, but a reliable conclusion about the particle size was only possible by *ex situ* SEM [4] or TEM [7] measurements. Soon afterwards, Mie scattering ellipsometry was used to measure the size of injected particles [8] as well as growing particles *in situ* [9, 10]. Recently, Greiner et al. introduced an Imaging Mie Ellipsometry technique, which is able to monitor the spatio-temporally resolved evolution of the particle growth in argon-acetylene plasmas [11].

Apart from the applications in industrial processing plasmas, dusty plasmas are also studied with respect to fundamental science. In this field of research, dust particles (usually melamine formaldehyde (MF) or other plastic particles of a well-defined size in the µm-range) are injected into chemically inert plasmas, where they acquire a highly negative electric charge of 10^3 e to 10^4 e. With an appropriate confinement, strongly coupled Coulomb systems can be formed, ranging from 2D layers [12, 13] over finite 3D clusters [14] to spatially extended 3D clouds [15, 16]. There, one exploits the advantage that the dust particles can be observed individually and, that due to their slow timescales, can be tracked in 3D throughout time, providing the full phase space information.

The MF particles generally used in fundamental studies offer a very narrow size dispersion and a highly spherical shape. Only few works exist where the size of MF particles has been investigated, since it is considered to be well-defined by the manufacturer. However, Liu et al. found the MF particles to be slightly smaller than specified by the manufacturer using TEM [17]. Swinkels et al. employed Mie ellipsometry to monitor the etching of MF particle clouds in oxygen plasmas [18] and Stoffels et al. investigated the etching of a single MF particle in an oxygen plasma by angular resolved Mie scattering [19]. Since most experiments on dusty plasmas use argon or other noble gases, chemical etching of the dust is not considered relevant. However, the outgassing of water, leading to a reduction of the MF mass density, has been observed by Carstensen et al. by a precise measurement of the dust resonance frequency over a long time [20]. There, the authors conjectured that the outgassing might be caused by an increased surface temperature of the dust particles in the plasma (which was observed by other groups [21, 22]). The assumption of a temperature-dependent outgassing is endorsed by thermogravimetry [20] and quadrupole mass filters measurements [23]. The dust size was, however, assumed to be constant in all of these experiments.

In this work, we developed a spatially resolving Mie Imaging technique, which is based on the angle-resolved measurement of the Mie scattering intensities. This method allows a precise determination of the dust size distribution in spatially extended dust clouds. In experiments featuring large, thermophoretically levitated and seemingly homogeneous dust clouds consisting of monodisperse MF particles, a somewhat segmented

structure of the dust cloud is visible (see e.g. our previous work [24] and, presumably, experiments from other groups with similar conditions [25]). Since this segmentation might be caused by differently sized particles, this issue will be addressed by Mie Imaging in this work.
Our Imaging Mie diagnostic is furthermore used to monitor the time evolution of the dust size distribution. The variation of the dust size with time is confirmed by *ex situ* microscopy of plasma-exposed dust. Further indirect evidence is found by measuring the dust plasma frequency over time and the response of the dust to different (thermophoretic) force fields.
In order to gain insight into the physical processes leading to the changes in dust size and mass, mass spectrometry has been used to identify possible signatures of dust outgassing or etching. Furthermore, the surface temperature of the dust particles has been measured using fluorescent dust particles and the chemical structure of MF dust was evaluated using FT-IR absorption.

II. EXPERIMENTAL SETUP

Our main experiments have been performed in a capacitively coupled radio frequency (ccrf) plasma that has a 360 ° optical access. Some supporting experiments have been carried out in a typical rf discharge chamber. In both cases, argon plasmas are ignited at 13.56 MHz with a gas pressure on the order of 10 Pa (measured by a capacitance vacuum gauge) and low plasma powers in the range of 1 to 10 W. The dust particles are stored in dispensers under vacuum conditions (the base pressure of the plasma chamber is approximately 0.1 Pa) prior to the experiments.

A. Main experimental setup

A symmetric parallel plate setup with temperature-controlled electrodes is used to confine spatially extended dust clouds (details in Ref. [24]). The circular electrodes with a diameter of 8 cm are separated by a 3 cm discharge gap and are operated in push-pull-mode. A volume-filling dust cloud is produced by using the thermophoretic force to compensate for gravity. Therefore, a temperature gradient is created in the neutral gas by heating the lower and cooling the upper electrode, resulting in an upwards directed thermophoretic force.
In order to perform angle-resolved measurements of the Mie scattering intensity, the plasma chamber is completely transparent by using a glass cylinder as the outer wall. A CCD camera is placed on a rotating stage (details in Ref. [26]), allowing to observe the dust cloud from any angle with respect to a stationary laser. The Mie scattering experiments described in Sec. III, the thermophoretic force field measurements (Sec. IV B) and the mass spectrometry (Sec. IV E) have been carried out in this device. A sketch of the plasma chamber and the rotating stage is shown in Fig. 1.

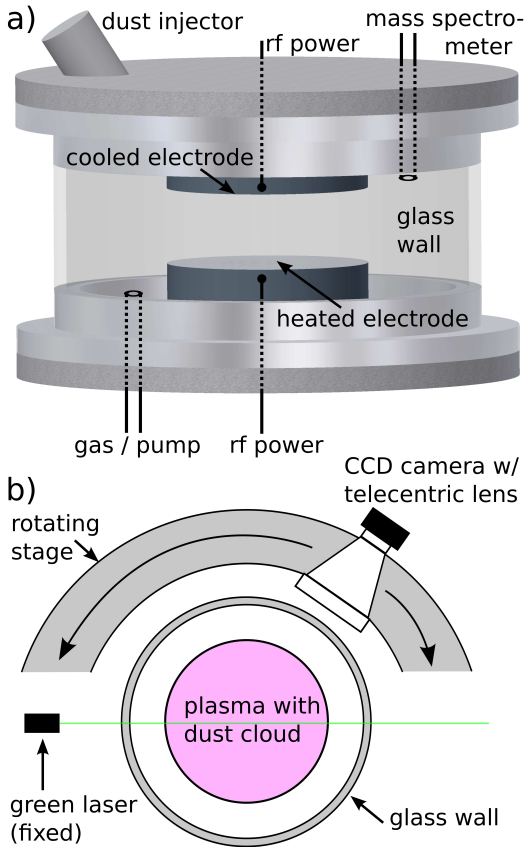

FIG. 1. Sketch of the symmetric plasma setup. a) front view of the plasma chamber. b) top view of the diagnostic setup for Mie Imaging.

B. Supporting experiments

This setup consists of an asymmetric discharge with a powered lower electrode (diameter of 170 mm), where the chamber walls act as the grounded electrode [14, 27]. This plasma chamber is used for the measurement of the resonance frequency of small dust clusters over time using the phase resolved resonance method of Carstensen et al. [20], which is described in Sec. IV C. Furthermore, the dust surface temperature measurements have been carried out in this setup. Also, particles have been collected from this device for *ex situ* microscopy (Sec. IV D).

III. ANGULAR RESOLVED MIE SCATTERING

For dust particles with a size of a few micron, the Mie scattering signal has a characteristic angular dependence [28]. With our diagnostic we aim to combine imaging techniques with the angle-resolved measurement of Mie scattering signals. The angular Mie scattering signals from a single particle have been used by Stoffels et al. to

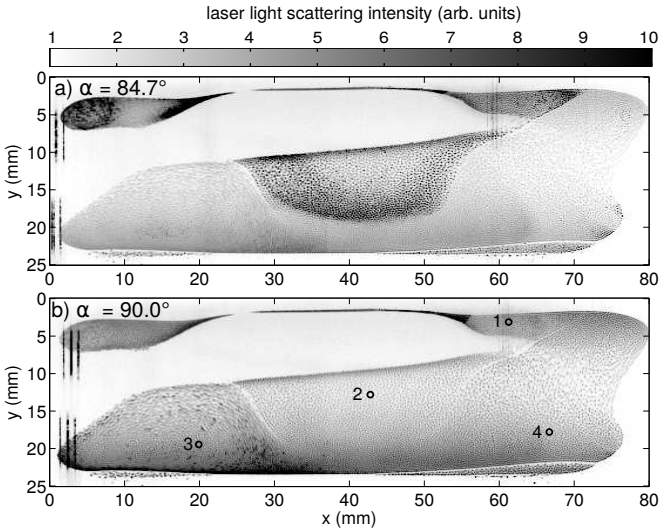

FIG. 2. Images of a typical dust cloud recorded from a) 84.7° and b) 90.0° (with respect to the laser slice). The laser light scattering intensity is shown in inverted grayscale. The vertical stripes at the left edge of the images are laser reflections.

measure the particle size evolution of this single MF particle being etched in an oxygen plasma [19]. In our setup with a completely transparent plasma chamber, we are able to observe the dust cloud from a wide angular space, as sketched in Fig. 1 b). To avoid too heavy optical distortion for the imaging, however, our measurements are limited to an angular range of 90°, stretching roughly from 45° to 135° with respect to the incident laser beam. For our Mie scattering experiments, we use highly spherical MF particles with a nominal radius of 1.775 µm and a refractive index of $n = 1.68$ (real part), as given by the manufacturer (Microparticles GmbH).

A thin slice of the dust cloud is illuminated by a vertical laser sheet (about 1 mm thick). The laser light has a wavelength of 532 nm and is linearly polarized in the horizontal plane. Hence, only the parallel component of the Mie scattering signal is measured. The scattered laser light is observed by a CCD camera, which is equipped with a telecentric lens and an optical filter to suppress the plasma light emission.

Two representative images of a typical dust cloud, taken from two slightly different angles, are shown in Fig. 2 in inverted grayscale. Besides the presence of the central void, the dust cloud appears to be segmented into different parts, which are separated by sharp intensity edges. Some segments of the dust cloud are particularly bright at a scattering angle of 84.7 ° (Fig. 2 a)), while others show a higher intensity at 90.0 ° (Fig. 2 b)). Observing the dust cloud from many different angles, we find that each segment of the dust cloud features a distinct dependence of the scattered intensity from the observation angle. To illustrate this fact, four representative parts of the dust cloud are further examined in Fig. 3. Each of the four arbitrarily chosen points (whose locations are

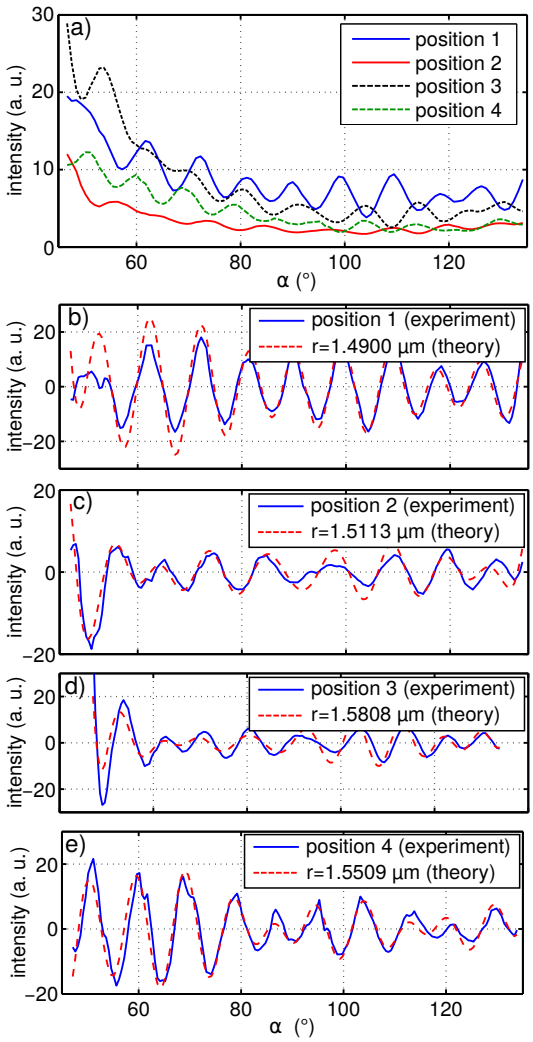

FIG. 3. a) Angular resolved scattering intensity for the four example points indicated in Fig. 2 b). In parts b) - e), each of the four graphs is shown separately and accompanied by the respective fit of the Mie scattering theory (with moving average subtracted).

indicated by small circles in Fig. 2 b)) resembles an area averaged over 5×5 pixels in the original images in order to enhance the data quality. In Fig. 3 a), the scattering intensity for each point is shown as a function of the observation angle. It is clearly visible that each graph has a distinct behaviour.

With all required parameters for Mie scattering at hand (laser wavelength and polarization, dust refractive index), we can deduce the particle size from the scattering signals in Fig. 3 a). Since the dust particle radius is now the only free parameter for the Mie scattering problem, it can be determined by least-square fitting the Mie theory signals to the experimental results.

We found that the intensity oscillations together with the angular positions of the intensity peaks is much more reliable than the actual scattering amplitudes, which are influenced by experimental uncertainties (e.g. small fluc-

tuations in the dust cloud, laser beam quality, CCD camera sensitivity). Hence, a moving average filter is applied to the angle-resolved scattering signals for each position, resulting in intensity oscillations with a zero mean value. Now, the radius is determined by fitting the Mie theory scattering signals (also with moving average subtracted). The results are shown in Fig. 3 b) - e) for each of the four selected positions separately. The Mie theory fits agree very well with the course of the individual experimental graphs. Surprisingly, the fitted radii differ by about 6 % with respect to each other, which is about three times larger than the standard deviation of the particle size given by the manufacturer. Furthermore, the particles are specified to have a mean radius of 1.775 µm and therefore seem to be considerably smaller in our measurement. Monitoring the dust size distribution over the course of a few hours, a drastic further reduction of the particle size is observed. In Fig. 4, the size distribution in the dust cloud from Fig. 2 is shown for different times after the dust injection at t_0 [with Fig. 4 a) corresponding to the situation in Fig. 2 and 3]. Besides the obvious reduction of the particle size, the overall shape of the dust cloud is also changing. This effect can be explained by the constant size (and mass) loss of the dust particles. As a result of such a process, the force balance between gravity (scaling with a^3) and the thermophoretic force (scaling with a^2) is disturbed. For shrinking dust particles, the thermophoretic force wins over gravity, leading to the accumulation of the dust in the upper part of the cloud.

Comparing the dust size in a specific area of the cloud over time, one can try to calculate a size loss rate. This value will not describe the actual loss rate of a single particle, but rather the size evolution of the dust particles in that area (which will not necessarily be the same particles over time, e.g. due to transport). The dust size at four arbitrarily chosen points (indicated in Fig. 4 c)) as a function of time is shown in Fig. 4 d). The dust size decreases with a roughly constant rate at all four locations. From 10 measurements over the course of about two hours (after more than two hours, all the dust is compressed in a flat layer at the upper sheath), we find an average size loss rate of 0.04 nm/s. This rate is almost as large as the etching rate for MF particles in oxygen plasmas, which was found to be in the range of 0.06 nm/s to 0.13 nm/s for plasma powers of a few Watts [18, 19].

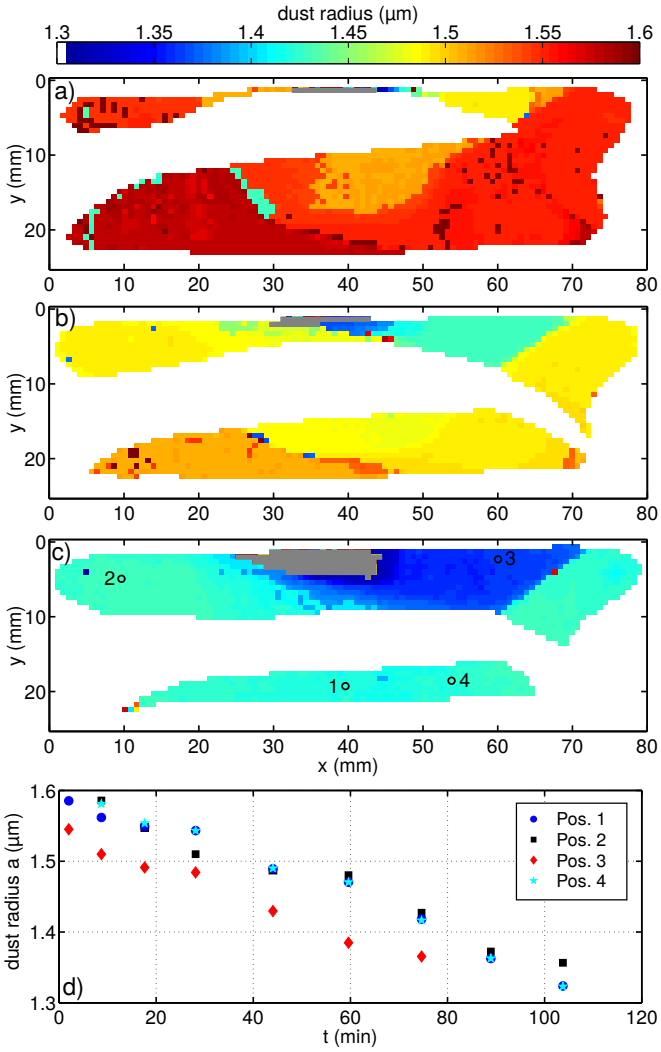

FIG. 4. Dust size distribution at different points in time with respect to the dust injection at t_0: a) $t_0 + 18$ min ; b) $t_0 + 44$ min , c) $t_0 + 75$ min. In the upper part of the dust cloud, a unidentifiable segment is getting bigger with time. This population seems to contain differently sized particles and is masked in gray color here. d) Dust size at the four locations indicated in part c) as a function of time.

IV. ADDITIONAL DIAGNOSTICS

The Mie Imaging results in the previous section strongly indicate that the dust particle size heavily decreases with time. Possible reasons may include chemical etching, sputtering, and outgassing. In order to evaluate the importance of each of these processes, additional experimental techniques have been employed. As a general approach, we assume that the dust radius a and the mass density ρ may both change over time.

For some experiments, the dust particles ware baked in an oven at $120 - 130\,^{\circ}$C prior to the experiments. This procedure has been proposed due to evidence of the outgassing of water from the MF particles in the plasma [20, 23]. With the baking process, most of the water bound in the MF is supposed to evaporate.

A. Ex situ microscopy

In order to verify the shrinking of dust particles in the plasma with a very reliable technique, dust particles have been examined with an optical video microscope before and after plasma exposure. Furthermore, the influence of

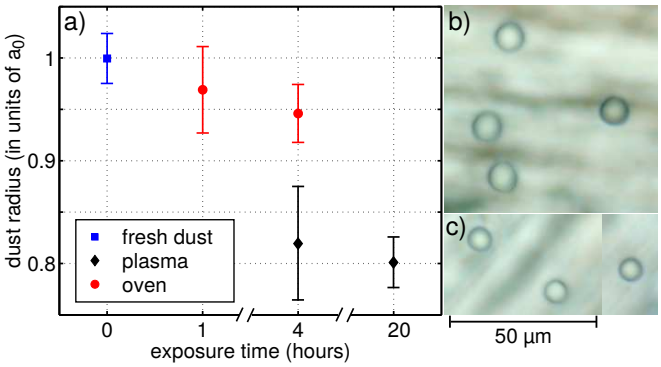

FIG. 5. a) Mean dust size obtained under the microscope for fresh, plasma-exposed and baked dust. Each data point is the result of averaging over up to 20 individual dust particles, with the standard deviation represented by the errorbars. For clarity, sample images of dust particles with a specified radius of $a_0 = 5.1$ µm under a microscope are shown for b) fresh dust and c) plasma-exposed dust.

oven-baking on the particle size is investigated. A typical image using a magnification of 500 is shown in Fig. 5 b) and c), where fresh and plasma-exposed particles are shown. The dust size is evaluated by fitting circles to the edge of the particles.

The resulting dust sizes are shown in Fig. 5 a), where each data point represents an average of all dust particles (typically 10 to 20) in the respective situation. The reference at $t = 0$ corresponds to unused, fresh dust particles. The oven-baked particles were exposed to a temperature of 120°C and are marked in red. These particles already show a slightly decreased size after baking, which accumulates to a shrinking of almost 6 % after 4 hours baking (with the size ratio of exposed dust (radius a) and fresh dust (radius a_0) determined as $a/a_0 = 0.945$). This leads to the conjecture that the dust particles contract due to the outgassing of volatile components such as water and formaldehyde.

For the plasma-exposed dust, a a more drastic change of the dust size is observed, with ratios of $a/a_0 = 0.82$ after 4 hours and $a/a_0 = 0.80$ after 20 hours. In these experiments, MF particles with a specified radius of 5.1 µm have been confined in the sheath of the asymmetric discharge (see Sec. II B) at an argon pressure of 20 Pa and a plasma power of 4 W. Surprisingly, the difference between 4 hours and 20 hours of plasma operation is quite small, indicating a saturation of the process that leads to the dust size reduction. However, the ratio a/a_0 agrees well with the values obtained from the Mie Imaging technique in the symmetric discharge.

B. Thermophoretic force fields

The dust size maps in Fig. 4 do not only reveal a decreasing dust size but also a shifting overall shape of the dust cloud. For a confined particle, the force balance results in a zero net force. For dust particles in the plasma volume (where the electric field is small), the vertical confinement is mainly influenced by the interplay between the gravitational force (pointing downwards) and the thermophoretic force (pointing upwards). Since both forces scale differently ($F_g \sim a^3\rho$ and $F_{th} \sim a^2$), a reduction of particle size or mass density will lead to the thermophoretic force gaining the upper hand over gravity. Hence, the dust will move upwards until another force compensates the excess of thermophoresis over gravity. This other force may be due to the electrostatic pressure of the dust cloud or, finally, the sheath electric field close to the upper electrode.

Therefore, the dust cloud shifts upwards as a whole (Fig. 4), and after a few hours of plasma exposure, the entire dust cloud is compressed into a thin layer at the upper sheath due to the drastic mass or size loss of the particles. Now, if the plasma is turned off, the sheath electric field instantly vanishes and the dust particles will be accelerated upwards due to the thermophoretic force being stronger than gravity. Because of friction of the dust with the neutral gas, the dust reaches terminal a velocity almost instantly. The force balance for the dust particles at the terminal velocity can be written as

$$F_g(a,\rho) + F_{th}(a) + F_n(a,v) = 0 \quad , \tag{1}$$

where F_n is the neutral gas friction, which depends on $F_n \sim a^2 v$ (with the dust velocity v). For this experiment, the temperature gradient in the neutral gas is set to a value where freshly injected dust particles with the radius a_0 and mass density ρ_0 are almost ideally well levitated after the plasma is switched off, due to $F_g(a_0,\rho_0) = -F_{th}(a_0)$. Combining the force balances for the plasma-exposed dust and the fresh dust, we find

$$\frac{a\rho}{a_0\rho_0} = 1 + \frac{C_1}{C_2} v \quad , \tag{2}$$

where C_1 and C_2 correspond to the coefficients for the neutral drag force and thermophoretic [29] force, respectively:

$$C_1 = \frac{32\, p\, \delta}{3\, v_n} \quad \text{and} \quad C_2 = \frac{-3.33\, k_b\, \nabla T}{\sigma} \quad . \tag{3}$$

Here, p, v_n and ∇T are the pressure, thermal velocity and temperature gradient of the neutral gas; $1 \le \delta \le 1.44$ is a geometric scattering coefficient and σ is the gas kinetic collision cross section.

In experiments similar to the situations in Sec. III, dust particles which have been exposed to the plasma for two hours, attain terminal velocities of about 25 mm/s after the plasma is switched off. Estimating $C_1/C_2 \approx 10$ s/mm for our conditions, this velocity corresponds to a ratio of $(a\rho)/(a_0\rho_0) \approx 0.75$. Even if a mass density loss due to outgassing is accounted for ($\rho/\rho_0 \approx 0.9$), this technique reveals a heavily decreasing dust size on the order of $a/a_0 \approx 0.8$.

In a different experiment involving five hours of plasma

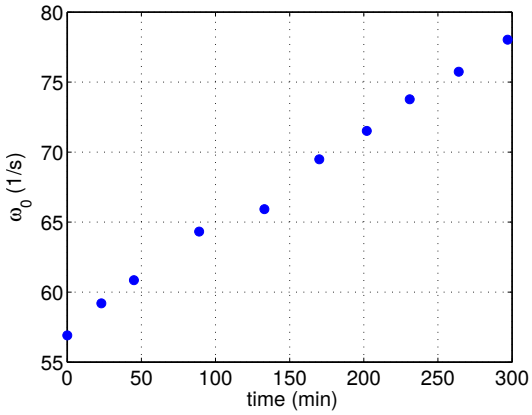

FIG. 6. Time evolution of the dust plasma frequency, measured with the phase resolved resonance method described in Ref. [20]. Over the course of 5 hours, the frequency increases by 37 %.

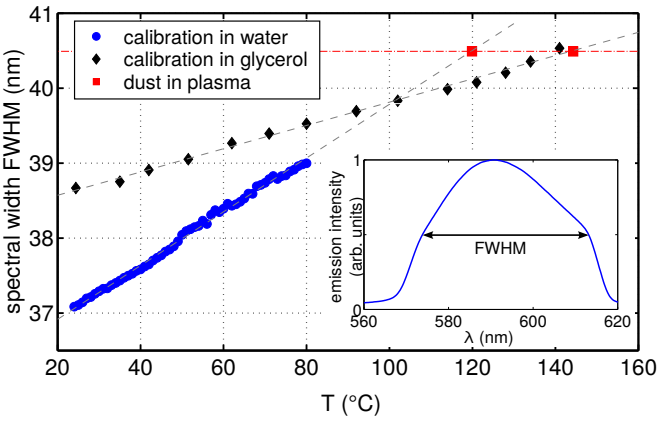

FIG. 7. Full width at half maximum of the fluorescence spectrum emitted by the Rhodamine B-doped dust particles. In the inset, a typical emission spectrum is shown.

exposure, an even more drastic effect was found. There, the particle attained velocities of about 50 mm/s, resulting in a ratio of $(a\rho)/(a_0\rho_0) \approx 0.5$.

C. Phase resolved resonance

To illustrate this further, we investigated the force balance for a small ensemble of dust particles located in the plasma sheath of the supporting discharge. There, the particles are vertically confined by the force balance between gravity and electric field force due to the sheath electric fields (thermophoresis is not used in this situation). If the electrode voltage is sinusoidally modulated with a low frequency, the dust particles behave as damped harmonic oscillators with an eigenfrequency ω_0, which is proportional to the dust's charge-to-mass ratio $\sqrt{q_d/m_d}$ [30].
Recently, Carstensen et al. established a very precise technique for the determination of relative changes in the dust particles' plasma frequency, called *Phase resolved resonance method* [20]. There, the authors found that dust plasma frequency of an MF particle confined in the sheath of an argon rf plasma increased by $5-6\,\%$ over the course of a few hours. Since the dust plasma frequency scales with $\sqrt{q_d/m_d}$, they concluded that during the measurement time the dust mass was reduced by $10-12\,\%$, assuming a constant size and therefore constant charge q_d. The most probable cause for this behaviour was reasoned to be the outgassing of water from the MF material. This assumption is supported by the temporal evolution of the dust plasma frequency, featuring a steep increase at the beginning, later turning into a slow saturation, and ultimately resulting in a constant eigenfrequency after 10 hours.
We adapted the phase resolved resonance method from Ref. [20] and found an even stronger effect in our experiments, which were performed in the asymmetric plasma chamber described in Sec. II B. The experimentally obtained dust plasma frequencies are presented in Fig. 6 and reveal a linear increase with time. After 5 hours, a total increase of 37 % is observed, corresponding to a relative change in the charge-to-mass ratio of

$$\frac{\omega^2}{\omega_0^2} = \frac{q}{m}\Big/\frac{q_0}{m_0} = \frac{a}{\rho a^3}\Big/\frac{a_0}{\rho_0 a_0^3} = \frac{a_0^2\rho_0}{a^2\rho} = 1.87 \quad .$$

Here, the relations $q \sim a$ and $m \sim \rho a^3$ have been used. This drastic result is probably not purely caused by a mass loss due to outgassing, as it was proposed in Ref. [20].

D. Evidence of outgassing or chemical processes

The process of water gassing out from the MF material strongly depends on the MF temperature [20, 23]. Often, the temperature of the dust particles confined in the plasma is assumed to be equal to the gas temperature, which is roughly at room temperature. At this temperature, no significant outgassing is expected. There are however a few works, where the dust material temperature in the plasma has been measured using fluorescent dye [21, 31] or phosphor particles [22].
Here, we employed the method described by Swinkels et al. [21], which uses MF dust with incorporated fluorescent dye (Rhodamine B), whose emission spectrum is temperature-dependent. First, two calibration measurement have been performed, where the fluorescent dust particles were dissolved in water and glycerol, respectively. The jars containing the solutions were placed on a heatable magnetic stirrer. The fluorescence has been excited by a green laser (532 nm) and was observed with a compact spectrometer. An optical bandpass filter suppressed the green laser light from the spectrometer.
The emission curves have been measured and the full widths at half maximum (FWHM) have been determined

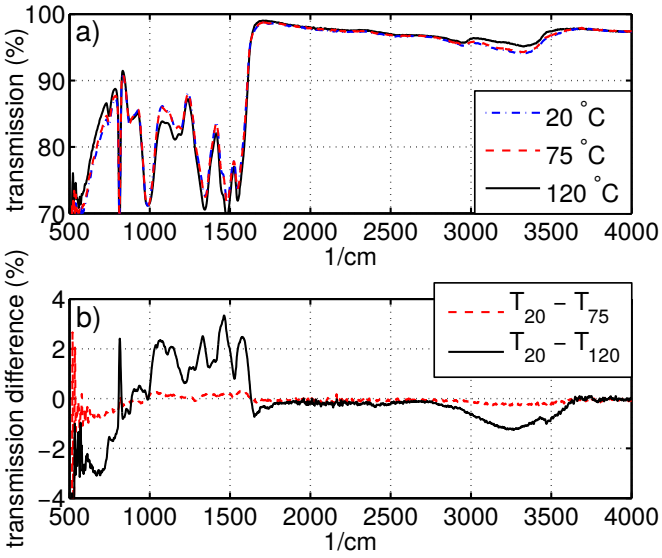

FIG. 8. a) FT-IR absorption spectra of untampered dust (20 °C) and baked dust at two different temperatures. b) difference of the transmission spectra with respect to the unheated dust.

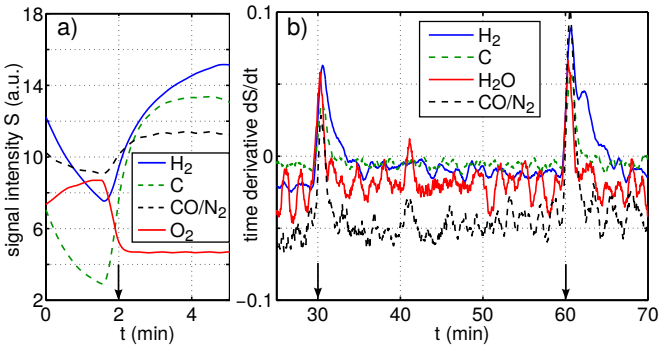

FIG. 9. a) Time evolution of four representative mass numbers measured with a quadrupole mass spectrometer. At t=2 min, the plasma is ignited. b) Time derivative of representative mass signals, emphasizing smaller changes. At t=30 min and t=60 min, dust is injected into the plasma.

as a function of the temperature, see Fig. 7. The FWHM is a reliable quantity for the temperature measurement from the emission spectra, since with increasing temperature the spectra become flatter and broader, while the overall shape of the emission curve does not change much (one sample spectrum is shown in the inset of Fig. 7). From the calibration curves of FWHM vs. temperature, a linear dependence is found for both solvents. The different slopes of the obtained calibration curves can probably be attributed to absorption by the solvents.

Now, the emission curve of fluorescent dust particles confined in the plasma sheath has been measured (using the asymmetric chamber described in Sec. II B). The same laser is used for excitation and a background spectrum of the plasma emission (without laser and fluorescence) is recorded. From the emission of the particles in the plasma, again the FWHM is determined and found as 40.5 ± 0.15 nm. Using the linear fits obtained from the calibration curves in Fig. 7, a dust temperature of $T = 119.8 \pm 4.4\,^{\circ}\mathrm{C}$ (calibration in water) and $T = 144.5 \pm 9.7\,^{\circ}\mathrm{C}$ (calibration in glycerol) is found. These values agree very well with results reported in Refs. [21, 31]. Reasons and possible mechanisms for the high dust temperature (compared to the neutral gas and the heated electrode, which are both below 40 °C) are discussed in Ref. [21]. In our situation, the energy influx due to the recombination of argon ions on the dust surface is thought to be the most important factor.

This elevated dust temperature will favour the outgassing of water and possibly formaldehyde (as stated by the manufacturer [32]). To verify the outgassing process, FT-IR absorption measurements have been performed with untampered dust as well as pre-baked dust, which has been in an oven at elevated temperatures for two hours. The absorption spectra in Fig. 8 a) reveal only a minor change when the dust was heated to 75 °C, but a stronger effect for the dust baked at 120 °C. To emphasize the effect of baking, the difference of the transmission spectra is shown in Fig. 8 b). The dip between 3000 cm^{-1} and 3500 cm^{-1} corresponds to the typical FT-IR absorption wavenumbers of water, while the changes at lower wavenumbers represent the chemical constituents of the MF material [33]. The decrease of the water absorption at higher temperature indicates that water has outgassed from the dust due to the baking. Furthermore, the chemical structure seems to be significantly altered by heating the dust to 120 °C.

E. Plasma mass spectrometry

The most probable causes for the decrease of dust size and mass in the plasma are chemical etching and the outgassing of volatile contents from the dust material. These processes naturally evoke a transport of water or organic chemical compounds from the dust material into the plasma. To analyse the composition of the gas in our plasma chamber, a quadrupole mass spectrometer for residual gas analysis has been used. Besides the argon feed gas, some residual molecules and atoms such as C, N, O, HO, H_2O, N_2, CO, O_2, CO_2 and others are found in the (dusty) plasma.

For the evaluation of the influence of the dust presence on the gas composition, the symmetric chamber (see Sec. II A) has been evacuated to the base pressure of about 0.1 Pa (using a rotary pump). After reaching base pressure, the argon flow is started and the plasma is switched on. Performing a time-resolved measurement of these characteristic masses, already a significant influence of the plasma operation on the gas contents is found. Igniting a plasma (at otherwise constant parameters) leads to a heavy increase of the H_2 signal and, to a smaller extent, to an increase of C and CO / N_2 (both $m = 28$), while the

O_2 signal decreases (due to dissociation in the plasma), as is depicted in Fig. 9 a). Switching the plasma off or reducing the plasma power leads to an opposite behaviour of these mass signals (increase of O_2, decrease of H_2, C and $CO\,/\,N_2$). This is also the explanation for the behaviour of the mass signals prior to plasma ignition in Fig. 9 a): the plasma was switched off earlier, some minutes before $t = 0$.
Now, a large amount of MF dust particles is injected into the plasma with an electromagnetic dust dispenser at $t = 30\,\mathrm{min}$ and $t = 60\,\mathrm{min}$. The injection results in an almost instantaneous increase of the signals for H_2, C, H_2O and $CO\,/\,N_2$, which is shown in Fig. 9 b). To emphasize the relative changes, the time derivative of the mass signals is plotted here. The narrow peaks of the time derivatives upon dust injection indicate a jump of the overall concentration of the respective mass numbers. This result further confirms that outgassing and/or chemical reactions take place.

V. DISCUSSION

The Mie Imaging technique presented in this work together with the additional diagnostics gives insight into the dust size distribution and its temporal evolution. In this last section, we will discuss these two main aspects.

A. Spatial dust size distribution

The de-mixing of differently sized particles in dusty plasmas is known to take place in situations involving binary mixtures with large size differences between the two species [34–36]. Now, our Mie Imaging method provides an excellent resolution, which allows to discriminate size differences of a few nm for micron-sized particles. The resulting dust size maps in Fig. 4 reveal a de-mixing of slightly differently sized particles, which results in a segmentation of the dust cloud. It is interesting to note that the dust size maps indicate a rather discrete dust size distribution instead of a smooth distribution, which is naturally expected [17]. However, since our Mie diagnostic reveals the dust sizes only in a thin 2D slice of the entire cloud, other dust sizes might be found in other parts of the cloud.
A general limitation concerning the spatial resolution of the dust size maps is given by the fact that we do not observe single dust particles but rather an ensemble of a few particles corresponding to a pixel in the camera images. Therefore, our Mie scattering technique is limited by the requirement for homogeneous dust populations in the area of investigation (typically 5×5 pixels, but the same applies for smaller averaging areas). Hence, the angle-resolved scattering signals from a heterogeneous part of the dust cloud, which contains particles of different size, cannot be interpreted with regard to Mie theory. Such parts of the dust cloud are shown in gray color in Fig. 4.
This limitation can however be used to estimate the timescale required for the de-mixing, which was found to be on the order of a few minutes for our supposedly monodisperse particles featuring only small size differences ($\Delta a/a \leq 10\,\%$). This can be inferred from a dust cloud, that has been confined in the plasma for at least 30 minutes (similar to the ones in Fig. 4), and subsequent injection fresh dust particles. Directly after injection, the observed Mie signal cannot be interpreted by dust particles of a unique size, indicating mixed populations. In some situations, it took up to 30 minutes to observe clear, unambiguous scattering signals. Hence, de-mixing might take a long time compared to most other dust processes. It should also be kept in mind that de-mixing in the plane perpendicular to the laser illumination cannot be observed by our diagnostic.
Finally, the validity of the absolute values for the dust size determined by Mie Imaging depends on the refractive index of the dust. We have used $n = 1.68$, as specified by the manufacturer [32]. However, the absolute size determined from Mie scattering does not match the size specified by the manufacturer, but is somewhat smaller (assuming a different value for n naturally affects the determined particle size). Nonetheless, the *relative* size differences shown in Fig. 4, and therefore the de-mixing phenomenon, are independent of the choice of the refractive index.

method	exposure	measured ratio	result
Mie scattering	$1\,h$ plasma	a/a_0	0.90
	$2\,h$ plasma	a/a_0	0.81
ex situ	$4\,h$ plasma	a/a_0	0.82
microscopy	$20\,h$ plasma	a/a_0	0.80
	$1\,h$ oven	a/a_0	0.97
	$4\,h$ oven	a/a_0	0.95
phase resolved	$2\,h$ plasma	$(a^2\rho)/(a_0^2\rho_0)$	0.75
resonance	$4\,h$ plasma	$(a^2\rho)/(a_0^2\rho_0)$	0.59
thermophoretic	$2\,h$ plasma	$(a\rho)/(a_0\rho_0)$	$0.75-0.80$
force field	$5\,h$ plasma	$(a\rho)/(a_0\rho_0)$	$0.50-0.60$

TABLE I. Size and mass density ratios obtained by different experimental techniques.

B. Temporal changes of dust size and mass

Besides the Mie Imaging technique, various additional experimental methods have been employed in this work to investigate the temporal changes of dust particle sizes. To draw a complete picture, the results of all experimental techniques are listed in Tab. I. For comparison, the kind (plasma or oven) and duration of the particle exposure is given in each situation.
The most unambiguous evidence of the dust particle size

loss in the plasma is given by the Mie scattering and the *ex situ* microscopy, since these techniques directly measure the (relative) particle size. Comparing the results from these two techniques, indicates that the size loss is mainly occurring in the first hours of plasma exposure, since the final ratio of $a/a_0 = 0.8$ found by microscopy after 20 h is observed by Mie Imaging already after 2 h. The size reduction is therefore supposedly a saturating process. Unfortunately, this cannot be further investigated by the Mie Imaging technique, since after more than two hours, the entire dust population is compressed in a thin layer below the upper electrode (see Sec. IV B). In this situation, no clear signal can be derived from Mie scattering theory, probably due to the mixing of different dust sizes. Furthermore, after a few hours in the symmetric discharge, the increasingly smaller and lighter dust cannot confined any more, and ultimately no dust is left in the plasma.

It might also be possible that the different experimental conditions for Mie Imaging and microscopy have influenced the size loss rate: For the microscopy, MF particles with a radius of $a_0 = 5.1\,\mu\text{m}$ were confined in the sheath of an asymmetric discharge, while the Mie scattering experiments were performed with smaller ($a_0 = 1.775\,\mu\text{m}$), thermophoretically levitated MF particles confined in the plasma volume of a symmetric discharge. Finally, it could be conjectured that the refractive index of the MF particles is not constant during plasma exposure. A change of the refractive index due to chemical reactions might lead to inaccurately determined dust sizes using Mie Imaging. While the dust size changes determined by Mie Imaging and microscopy are very reliable, the last two techniques in Tab. I provide more indirect, but still very profitable evidence. Assuming a reduction of the mass density of $\rho/\rho_0 = 0.9$ [20], the phase resolved resonance experiments result in $a/a_0 \approx 0.9$ after 2 hours and $a/a_0 \approx 0.8$ after 4 hours. The results of the force field experiments, again assuming $\rho/\rho_0 = 0.9$, also yield $a/a_0 \approx 0.85$ after 2 hours, and a more drastic value of $a/a_0 \approx 0.6$ after 5 hours of plasma exposure.

Comparing the different experimental approaches, the investigations in the symmetric plasma chamber with the volume-filling, thermophoretically levitated dust clouds tend to result in a higher size loss rate than the experiments on small dust ensembles in the asymmetric discharge. It could be conjectured that this might be to a self-enhancing effect. More dust particles release more volatile gases by outgassing, which can dissociate into oxygen radicals. The oxygen radicals can then, in turn, chemically etch the dust and therefore further reduce its size and mass.

This assumption on the mechanism behind the changing dust size and mass is supported by the mass spectrometry results (see Sec. IV E), where an instant increase of characteristic mass signals is observed upon dust injection. The initial outgassing, which is known to be temperature-dependent [20, 23, 32], is to be expected from the fluorescence-based temperature measurements, which revealed a dust temperature of about 125°C (see Sec. IV D). Furthermore, baking of unused MF particles was found to lead to the outgassing of water and other organic compounds. Plasma-related mechanisms such as sputtering by argon ions can probably be neglected in our experiments, since the dust potential is not larger than 10 V (with respect to the plasma potential), leading to a low energy of impinging argon ions. A basic calculation for the sputter rate in a comparable argon plasma is presented in Ref. [20], where the authors conclude that the argon sputter rate is orders of magnitude too low to account for the dust mass reduction. The same reasoning applies to our experiments.

VI. SUMMARY

In this work, we have presented a Mie Imaging technique which provides the spatially resolved size distribution of dust particles confined in an inert argon plasma. The high resolution of the dust size determination is achieved by measuring the Mie scattering signal angle-resolved over a wide angular range. Our measurements of spatially extended dust systems reveal a segmented structure of the dust clouds, where each segment contains a homogeneous population of dust particles with a distinct size. Since seemingly monodisperse particles are injected into the plasma, a self-excited de-mixing phenomenon is observed even if the size differences between the particles are very small ($\Delta a/a \leq 10\,\%$).

Observing the particle size distribution over time reveals a constantly decreasing dust size. This effect has been confirmed by *ex situ* microscopy of dust particles collected after plasma exposure. Further evidence of changes in the dust size and mass has been obtained from thermophoretic force field measurements and investigations of the dust particles' resonance frequency.

The physical processes behind this phenomenon have been evaluated by different approaches: Mass spectrometry of the plasma indicated that the injection and presence of dust particles in the plasma increases the concentration of impurities in the argon plasma (notably H_2, C, H_2O, CO/N_2). Furthermore, fluorescence-based temperature measurements of the dust particles' surface temperature in the plasma revealed elevated values of more than 100 °C. Such a high temperature was found to result in the outgassing of water and possibly organic constituents of the dust material by FT-IR absorption spectroscopy.

We therefore conclude that a combined action of outgassing of volatile constituents from the dust material and chemical etching due to impurities (possibly oxygen radicals) reduces the dust size and mass during confinement in the plasma. This result is of high importance for many experiments with dusty plasmas, which often use particles made of melamine formaldehyde or other plastics. We recommend either to regularly replace the dust in experiments or to account for the size and mass reduction in the data analysis.

ACKNOWLEDGMENTS

We like to thank F. Lawrenz (University Greifswald) and S. Peglow (INP Greifswald) for assistance with the microscopy and the FT-IR absorption measurements, respectively. Financial support from the German Aerospace Center DLR, contract No. 50WM1138 and from the Deutsche Forschungsgemeinschaft via SFB-TR24 project A3 is gratefully acknowledged.

[1] P. K. Shukla and A. A. Mamun, *Introduction to Dusty Plasma Physics* (Institute of Physics Publishing, Bristol, 2002).

[2] V. E. Fortov and G. E. Morfill, *Complex and Dusty Plasmas: From Laboratory to Space* (CRC Press, 2009).

[3] A. Bouchoule, *Dusty Plasmas: Physics, Chemistry and Technological Impacts in Plasma Processing* (John Wiley & Sons, 1999).

[4] G. S. Selwyn, J. Singh, and R. S. Bennett, J. Vac. Sci. Technol. A **7**, 2758 (1989).

[5] G. M. Jellum and D. B. Graves, Journal of Applied Physics **67**, 6490 (1990).

[6] P. R. i Cabarrocas, Y. Djeridane, T. Nguyen-Tran, E. V. Johnson, A. Abramov, and Q. Zhang, Plasma Physics and Controlled Fusion **50**, 124037 (2008).

[7] A. Bouchoule and L. Boufendi, Plasma Sources Science and Technology **2**, 204 (1993).

[8] K. Tachibana, Y. Hayashi, T. Okuno, and T. Tatsuta, Plasma Sources Science and Technology **3**, 314 (1994).

[9] Y. Hayashi and K. Tachibana, Jpn. J. Appl. Phys. **33**, 804 (1994).

[10] C. Hollenstein, J. L. Dorier, J. Dutta, L. Sansonnens, and A. A. Howling, Plasma Sources Science and Technology **3**, 278 (1994).

[11] F. Greiner, J. Carstensen, N. Köhler, I. Pilch, H. Ketelsen, S. Knist, and A. Piel, Plasma Sources Science and Technology **21**, 065005 (2012).

[12] J. H. Chu and L. I, Phys. Rev. Lett. **72**, 4009 (1994).

[13] H. Thomas, G. E. Morfill, V. Demmel, J. Goree, B. Feuerbacher, and D. Möhlmann, Phys. Rev. Lett. **73**, 652 (1994).

[14] O. Arp, D. Block, A. Piel, and A. Melzer, Phys. Rev. Lett. **93**, 165004 (2004).

[15] G. E. Morfill, H. Thomas, U. Konopka, H. Rothermel, M. Zuzic, A. Ivlev, and J. Goree, Phys. Rev. Lett. **83**, 1598 (1999).

[16] A. P. Nefedov, G. E. Morfill, V. E. Fortov, H. M. Thomas, H. Rothermel, T. Hagl, A. V. Ivlev, M. Zuzic, B. A. Klumov, A. M. Lipaev, V. I. Molotkov, O. F. Petrov, Y. P. Gidzenko, S. K. Krikalev, W. Shepherd, A. I. Ivanov, M. Roth, H. Binnenbruck, J. A. Goree, and Y. P. Semenov, New Journal of Physics **5**, 33 (2003).

[17] B. Liu, J. Goree, V. Nosenko, and L. Boufendi, Physics of Plasmas **10** (2003).

[18] G. H. P. M. Swinkels, E. Stoffels, W. W. Stoffels, N. Simons, G. M. W. Kroesen, and F. J. de Hoog, Pure and Applied Chemistry **70**, 1151 (1998).

[19] W. W. Stoffels, E. Stoffels, G. H. P. M. Swinkels, M. Boufnichel, and G. M. W. Kroesen, Phys. Rev. E **59**, 2302 (1999).

[20] J. Carstensen, H. Jung, F. Greiner, and A. Piel, Phys. Plasmas **18**, 033701 (2011).

[21] G. H. P. M. Swinkels, H. Kersten, H. Deutsch, and G. M. W. Kroesen, Journal of Applied Physics **88**, 1747 (2000).

[22] H. R. Maurer, R. Basner, and H. Kersten, Contributions to Plasma Physics **50**, 954 (2010).

[23] J. Pavlu, A. Velyhan, I. Richterova, Z. Nemecek, J. Safrankova, I. Cermak, and P. Zilavy, Plasma Science, IEEE Transactions on **32**, 704 (2004).

[24] C. Killer, G. Bandelow, K. Matyash, R. Schneider, and A. Melzer, Phys. Plasmas **20**, 083704 (2013).

[25] C. Schmidt, O. Arp, and A. Piel, Phys. Plasmas **18**, 013704 (2011).

[26] C. Killer, M. Himpel, and A. Melzer, Review of Scientific Instruments **85**, 103711 (2014).

[27] A. Schella, T. Miksch, A. Melzer, J. Schablinski, D. Block, A. Piel, H. Thomsen, P. Ludwig, and M. Bonitz, Phys. Rev. E **84**, 056402 (2011).

[28] H. van de Hulst, *Light Scattering by Small Particles* (Dover, 1981).

[29] H. Rothermel, T. Hagl, G. Morfill, M. Thoma, and H. M. Thomas, Phys. Rev. Lett. **89**, 175001 (2002).

[30] A. Melzer, T. Trottenberg, and A. Piel, Phys. Lett. A **191**, 301 (1994).

[31] J. E. Daugherty and D. B. Graves, Journal of Vacuum Science & Technology A **11**, 1126 (1993).

[32] *Microparticles GmbH*, personal communication.

[33] D. Wang, X. Zhang, S. Luo, and S. Li, Advances in Materials Physics and Chemistry **2**, 63 (2012).

[34] M. Mikikian, L. Boufendi, A. Bouchoule, H. M. Thomas, G. E. Morfill, A. P. Nefedov, V. E. Fortov, and the PKE-Nefedov team, New Journal of Physics **5**, 19 (2003).

[35] G. E. Morfill, U. Konopka, M. Kretschmer, M. Rubin-Zuzic, H. M. Thomas, S. K. Zhdanov, and V. Tsytovich, New Journal of Physics **8**, 7 (2006).

[36] A. V. Ivlev, S. K. Zhdanov, H. M. Thomas, and G. E. Morfill, EPL (Europhysics Letters) **85**, 45001 (2009).